NEUTRON DETECTION WITH SiC DETECTORS

YLENIA ŽIBER

Fakulteta za matematiko in fiziko
Univerza v Ljubljani

As the supply of ^{3}He diminishes, a need for neutron detectors without the typical ^{3}He-technology has arisen. Neutron detectors capable of detecting neutrons from fissile material are used to discover and inspect nuclear warheads and to prevent illicit trafficking of radiological materials. In recent years, semiconductor detectors have become most popular, especially those made from materials with a wide band gap like silicon carbide (SiC). The wide band gap at room temperature gives good spectral resolution in comparison to other semiconductor detectors (High Purity Germanium-HPGe) that require almost cryogenic temperatures.

SiC semiconductor devices are widely used in power electronics, especially the easily fabricated 4H-SiC crystal. They have good spectral resolution at room temperature and have a high radiation tolerance. To detect neutrons, a layer of converter material is added to the detector. In the converter material charged particles are created from neutron reactions and detected in the SiC detector. Different materials can be used depending on the neutron energy spectrum of interest. For the detection of thermal neutrons, ^{10}B and ^{6}Li are typically used. Such detectors have been studied extensively, including an ongoing research and development effort with experimental testing at the Jožef Stefan Institute (JSI) TRIGA Mark II. research reactor.

DETEKCIJA NEVTRONOV S SiC DETEKTORJEM

Za detekcijo nevtronov se trenutno najbolj uporabljajo plinski ^{3}He detektotji, vendar se zaloga ^{3}He na Zemlji zmanjšuje. Posledično, se je začelo iskati načine detekcije nevtronov brez uporabe ^{3}He-tehnologije. Detektorji nevtronov, ki lahko zaznajo nevtrone iz fisijskega materiala, se uporabljajo za preverjanje jedrskih bojnih glav ali za preprečevanje ilegalnega prevažanja radiološkega materiala. V zadnjih letih so postali najbolj priljubljeni polprevodniški detektoji, predvsem tisti, izdelani iz materialov s široko pasovno vrzeljo. Vedno bolj uporabljen je material silicijev karbid (SiC), saj ima za razliko od drugih polprevodnikov (germanij), široko pasovno vrzel že pri sobni temperaturi. Ta lastnost omogoča dobro spektralno resolucijo brez potrebe po hlajenju detektorja.

SiC polprevodniške naprave se pogosto uporabljajo v močnostni elektroniki. Zaradi preproste izdelave se najpogoste uporablja kristal 4H-SiC. Te naprave imajo dobro spektralno ločljivost pri sobni temperaturi in visoko toleranco na sevanje. Nevtrone lahko SiC polprevodnik zazna preko konverterskega materiala, saj v njem preko nevtronskih reakcij nastajajo nabiti delci. Izbira materiala za konverter je odvisna od nevtronskega energijskea spektra, ki nas zanima. Za detekcijo termičnih nevtronov se običajno uporabljata ^{10}B in ^{6}Li. Takšni detektorji so že obsežno raziskani tudi na Inštitutu Jožefa Stefana (IJS), kjer razvijajo detektorje na podlagi simulacij in meritev na raziskovalnem reaktorju TRIGA Mark II.

1. Introduction

The use of devices capable of detecting neutrons has expanded from fundamental research [19, 15] or inspection of nuclear warheads to the prevention of illicit trafficking of radiological materials, primarily through the screening of cargo at borders [8]. Considering the imminent shortage of ^{3}He available on Earth, detectors based on semiconductor technologies are under consideration for neutron detection.

The main advantages are low operating bias, small detector sizes, production yield, and gamma discrimination of such detectors. The main disadvantage is lower sensitivity in comparison to ^{3}He detectors. Silicon carbide (SiC) is nowadays used in power electronics [14], but devices with higher reliability and overall performance are required for security applications. A wide-gap semiconductor such as SiC can provide these specifications due to its thermal and mechanical stability. SiC-based detectors are strong candidates for use in particle detection under harsh conditions, especially at high temperatures and radiation fields, due to their radiation hardness, high signal to noise ratio, and excellent neutron/gamma discrimination for pulsed radiation [9].

In this paper I will be presenting SiC semiconductor detectors for neutron detection purposes, starting from Section 2. where SiC semiconductor detectors are described in general. In Section 3.

some SiC properties are presented that impact the semiconductor detector, while Section 4. describes the process of using SiC detectors as neutron detectors. In this paper the emphasis is on converter materials for the detection of various neutron spectrum sections. A prototype detector and detection system are presented in Section 5. Finally, conclusions are drawn in Section 6.

2. SiC semiconductor detector

In a crystalline material, the periodic lattice determines the allowed energy bands in which the electrons are confined. In a semiconductor, the allowed energy gaps are separated by a gap of forbidden energies. The lower band is called the valence band and consists of outer shell electrons bound to specific lattice sites. In the case of silicon, these electrons are part of the covalent bonds that constitute the interatomic forces of the crystal. The conduction band is the next highest band in which electrons can move freely. The size of the gap between the bands is determined by the material itself. If the gap is very large, the material is classified as an insulator. In contrast, metals have no gaps between the bands and are called conductors.

Thermal energy can excite an electron from the valence band into the conduction band. In the excitation process a vacancy is left in the valence band which, in conjunction with electron transfer, is called an electron-hole pair. By applying an electric field to the material, both holes and electrons start moving, holes in the direction of the electric field and electrons in the opposite direction.

Because of the small band gap in semiconductors, a large number of charge carriers can be achieved per unit energy loss of the ionizing particle. Typical values for band gaps are $E_g = 1.14$ eV for ^{28}Si and $E_g = 0.67$ eV for ^{72}Ge. The energy loss per length traveled in material is much higher in solid-state detectors in comparison to gaseous detectors, which allows for sufficiently high signals in solid detectors of small dimensions. Semiconductors are mechanically rigid and can be designed to be self-supporting.

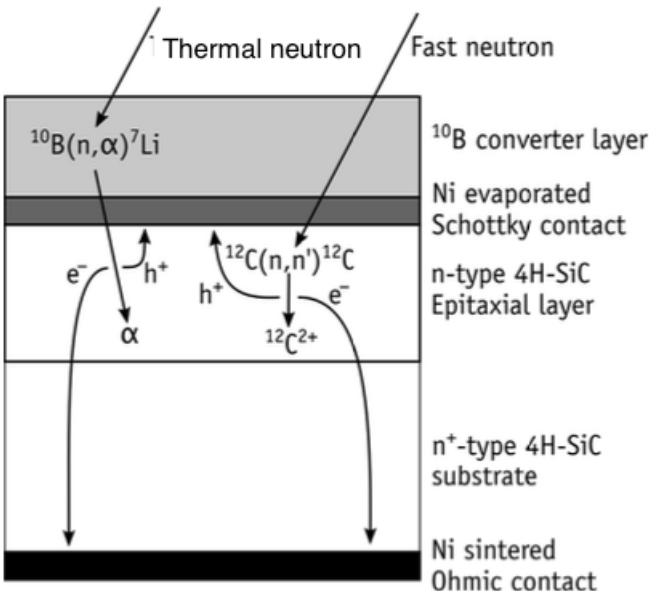

Figure 1. A schematic design SiC Schottky barrier diode suitable for neutron detection, with a converter layer over the front contact to improve sensitivity to thermal neutrons due to the presence of a nuclide with high thermal cross-section for (n,α), (n,p), (n,t) or other similar reactions. In this case there is a ^{10}B converter. Picture adapted from article [4].

Typically, a semiconductor detector is a large p-n type semiconductor diode operated in reverse bias. The type is defined by the majority of charge carriers released in a portion of the material.

N-type semiconductors have electrons as the main charge carriers in the conduction band, while the p-type semiconductors have holes in the valence band. In p-n semiconductor junctions electrons diffuse from the n-type material into the p-type material and holes diffuse the opposite way. Due to recombination, a depletion region in the vicinity of the junction appears. This depletion region can serve as a radiation detector. To increase the size of the depletion region, the diode is operated under reverse bias [10].

However, a typical SiC-based detector has the structure of a Schottky barrier diode (SBD), in which the junction is formed between a metal and a semiconductor (instead of a semiconductor-to-semiconductor junction as in conventional diodes), usually of the n-type because they are easier to fabricate [12]. A potential energy barrier, the Schottky barrier, is formed by the junction. A typical SBD can be seen in Figure 1.

3. SiC properties

The SiC compound can form different structures with a common stoichiometry, called polymorphs, which are stacked along a crystalline direction. The modifications can differ only in the stacking sequence. This property is called polytypism. In SiC, stacking occurs along the $\langle 0001 \rangle$ direction of the hexagonal close-packed lattice. Each aligned dimer is stacked to form atomic bilayers of type A, B, or C, as shown in Figure 2.

In principle, there are an infinite number of combinations, but only a few are of acceptable structural stability, namely (AB), (ABC), (ABCB), and (ABCACB). In most of the literature, the Ramsdell's notation [18] is used to describe these polytypes, which are referred to as $2H$, $3C$, $4H$ and $6H$ respectively. The number represents the number of SiC bilayers per unit cell and the letter indicates the lattice system (H-hexagonal, C-cubic). The width of the band gap is different for each structure. Some experimental values can be seen in Table 1.

The active layer of a SiC detector is grown by homoepitaxy, a process in which new crystalline layers are formed by material deposition with well-defined layer orientations on a substrate of the same material. The material of choice for applications in power devices, used as a switch, is $4H$-SiC, because its band gap is very high and the quality of the SBD resulting from homoepitaxy is very good [23].

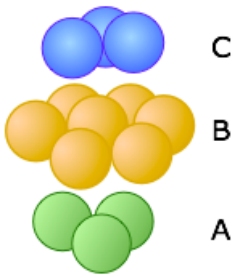

Figure 2. Possible stacking sites (A, B or C) for the Si–C crystal. Picture from [4].

Table 1. Experimental values for the band gap width E_g at cryogenic temperatures and room temperatures for different SiC polytypes [3, 23].

	$3C$-SiC	$6H$-SiC	$4H$-SiC	$2H$-SiC
E_g [eV], cryogenic T [3]	2.39	3.02	3.26	3.33
E_g [eV], room T of $T = 300$ K [23]	2.36	3.08	3.23	/

4. Neutron detection

General requirements for neutron detectors for monitoring applications are detection efficiency (the fraction of detected neutrons, usually expressed as a percentage), response linearity, long-term stability, background discrimination against gamma rays, and radiation hardness.

Since neutrons are neutral particles, they can only be detected indirectly in a semiconductor detector. We have two approaches to neutron detection. The first is to detect particles that are created after the neutron interaction with the detector materials (Si, C). The second is to add a converter layer, which I will define later in the paper. In a SiC crystal, the most probable interactions with fast neutrons ($E_n > 10$ MeV) are elastic and inelastic recoil scattering of ^{12}C(n,n')^{12}C or ^{28}Si(n,n')^{28}Si [7]. In these reactions, part of the energy and momentum of the incident neutron is transferred to ^{28}Si and ^{12}C nuclei. An atom can be knocked from the crystal if neutrons transfer sufficient kinetic energy to the atoms. A signal can be detected as a heavy ion moving through the depleted region, producing electron-hole pairs along the way, or as a permanent point defect. An example of the ^{12}C(n,n')^{12}C reaction is shown in Figure 1 on the right, where $^{12}C^{+}$ represents a recoil ion struck by a fast neutron, h^{+} represents holes, and e^{-} represents electrons.

The converter material improves the sensitivity of a neutron detector by emitting more detectable particles and is placed over the front contact. It consists of a layer of nuclei with a large scattering cross-section for the neutrons of interest (thermal, epithermal, or fast). The neutron reaction results in recoil ions that create electron-holes in the depletion region of the SBD. Since the air between the converter and the detector stops emitted charged particles, vacuum is needed for more accurate measurements.

The thickness of the converter material impacts the performance of the detector. If the material is too thin, there will be little interaction between the neutrons and the converter material, but the reaction products can easily reach the SiC and be detected there. On the other hand, a thicker converter may produce more interactions, but many of the products will be absorbed before they reach the SiC detector. It is important to optimise the thickness of the converter layer to achieve greater detection performance. When designing a new detector, the optimal converter thicknesses can be determined by Monte Carlo particle transport calculations. The detector and converter geometry and material composition is modelled explicitly using Monte Carlo particle transport codes such as MCNP [1], SERPENT [2], etc. and quantities such as energy deposition rates in the SiC detector due to incident charged particles from the converter are calculated.

Based on the optimised thickness, the converter can be prepared by calculating the required material mass m as $m = \rho A d$, where A is the detector area. Converters can be prepared as thin films by vacuum evaporation, sputtering or direct deposition of material in solution form. Materials suitable as substrates have low neutron absorption cross-sections in order to maximize the reaction rates in the converter materials themselves. Typically, aluminium plates are used for this purpose [13] as it has a very low absorption cross-section for neutrons, which is ideal for neutron measurements.

Depending on the desired neutron energy range, different converter materials are employed. Detection of thermal neutrons can be achieved with a converter layer rich in isotopes with a large effective cross-section for neutrons with an energy of about $k_B T$ at room temperature (corresponding to about 25.3 meV), where k_B is the Boltzmann constant. Similar to fission chambers, the most common isotopes are ^{10}B or ^{235}U. In addition, ^{6}Li is also used. From Table 2 it can be seen that materials such as ^{10}B, ^{235}U and ^{6}Li have much higher absorption cross-sections for thermal neutrons than ^{28}Si and ^{12}C.

The relevant reactions for ^{6}Li and ^{10}B are ^{6}Li(n,t)^{4}He and ^{10}B(n,α)^{7}Li, respectively. A possible device architecture is shown in Figure 1 with an implemented ^{10}B converter layer [4]. At first glance,

Table 2. The absorption cross-sections for a thermal neutron with kinetic energy E_n=25.3 meV for some materials [20].

	^{10}B	^{235}U	^{6}Li	^{28}Si	^{12}C
σ [barn]	938	3843	681	0.17	0.00353

one might assume that the detector response is higher for ^{10}B than for ^{6}Li because the effective cross-section of ^{10}B is about four times larger than that of ^{6}Li, but the response also depends on other factors, including the penetration depth of the reaction products into the depletion region. In this regard, the reaction products of ^{6}Li(n,t)α with kinetic energies of 2.05 MeV for alphas and 2.73 MeV for tritons, can generate more excitations than the alphas and $^{7}Li^{+}$ ions with 1.47 MeV and 0.84 MeV resulting from the reaction on ^{10}B [11].

Despite a significant volume of work on the general topic of semiconductor neutron detectors, only very few papers describe the applications of converting materials other than ^{6}Li or ^{10}B. Numerical studies have been published with ^{235}U used as a thermal neutron converter and ^{237}Np and ^{232}Th used as epithermal/fast neutron converters for semiconductor detectors, with nuclear fission being the "active" conversion reaction [6]. Fission fragments have energies 100 times higher than the charged particle energy range, which is referenced to charged particles emitted from neutron reactions, and may cause premature radiation damage to the semiconductor material. In the context of neutron capture therapy for the treatment of cancer, the ^{33}S(n,α) reaction is being studied [16] and it is of interest because of the possibility of exploiting epithermal and fast neutrons to enhance the delivered dose to the tumour and/or detector.

Because of the high scattering reaction cross-section of hydrogen, materials with high amount of hydrogen are some of the most effective converters. They also have a large recoil penetration depth of H^{+} into the semiconductor layer. Compared with other materials, these types of converters, such as polyethylene, have high conversion efficiency [21], but they usually cannot withstand a harsh radiation environment and/or high temperatures [22].

The selection for converters of fast neutrons can be made by the calculations of reaction rates with total cross-sections, as

$$R = \int \sigma(E)\phi(E)\, dE, \tag{1}$$

where σ is the reaction cross-section and ϕ is the neutron flux. In recent research carried out at the Jožef Stefan Institute, a selection process was made based on calculated reaction rates for 557 isotopes from the nuclear data library ENDF/B- VIII.0 [5]. By selecting reactions of interest such as (n,p), (n,d), (n,t), (n,^{3}He), (n,α), (n,t2α) and elastic scattering on hydrogen, a selection of possible reactions for the detection of fast neutrons has been made, which can be seen in Table 3 [24].

An interesting candidate converter material is ^{22}Na, offering sensitivity to thermal neutrons, whose calculated (n,p) reaction rate is an order of magnitude higher than the (n,p) reaction rate for ^{3}He. The major drawback is the radioactivity of ^{22}Na with a half life of 2.602 years.

Reactions produced predominantly by fast neutrons can be identified by the energies at which the integral of the reaction rate is 50 % of the total reaction rate (E 50 %). The isotopes ^{40}Ca, ^{58}Ni, ^{39}K and ^{35}Cl with E 50 % energies in the range of several MeV are the most promising and solid at room temperature. In contrast, reactions with a small value of E 50 %, about 45 meV, are predominantly sensitive to thermal neutrons. Figure 3 shows the cross-sections for reactions produced predominantly by fast neutrons.

Table 3. Calculated reaction rates with highest values for different isotopes and neutrons to charge particle producing the reactions. The energy at which the integral of the reaction rate is 50 % of the total reaction rate is represented in E 50 % (adapted from [24]). Reactions with a small value of E 50 % are predominantly sensitive to thermal neutrons, reactions produced predominantly by fast neutrons have a bigger value of E 50 %.

Isotope	Reaction	Reaction rate per neutr. src. par.	E 50% [MeV]	Natural abundance [%]	Radioactive
H	Elastic scattering	$8.98{\cdot}10^{-5}$	$1.067{\cdot}10^{-7}$	99.98	stable
22-Na	(n,p)	$4.34{\cdot}10^{-2}$	$4.567{\cdot}10^{-8}$	traces	2.602 y
40-Ca	(n,p)	$3.47{\cdot}10^{-7}$	4.48332	96.941	stable
58-Ni	(n,p)	$3.45{\cdot}10^{-7}$	4.53248	68.077	stable
39-K	(n,p)	$3.39{\cdot}10^{-7}$	3.46221	93.258	stable
35-Cl	(n,p)	$3.24{\cdot}10^{-7}$	2.99003	76	stable
6-Li	(n,t)	$1.41{\cdot}10^{-3}$	$4.543{\cdot}10^{-8}$	7.59	stable
10-B	(n,α)	$5.78{\cdot}10^{-3}$	$4.540{\cdot}10^{-8}$	20	stable
33-S	(n,α)	$1.13{\cdot}10^{-6}$	0.15735	0.75	stable
22-Na	(n,α)	$4.41{\cdot}10^{-5}$	$4.642{\cdot}10^{-8}$	traces	2.602 y

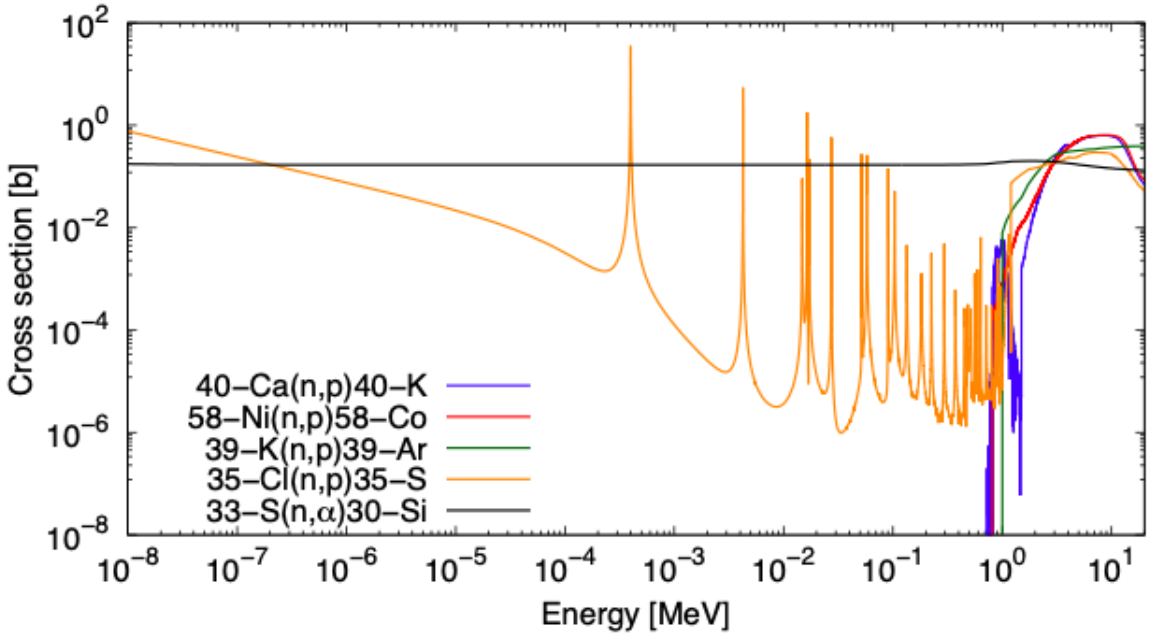

Figure 3. Cross-sections for reactions mainly produced by fast neutrons from the ENDF/B-VIII.0 nuclear data library. Picture from article [24].

5. Neutron detector prototype

The prototype detectors have an n-type 4H-SiC SBDs with different active layer thicknesses and dopant concentrations. The lateral dimensions are 1 mm × 1 mm. The active thickness used to obtain the results presented in this paper is 69 µm. The SBDs are surface-mounted onto chip carriers with a wire-bonded electrical contact [17]. The chip carriers are enclosed in 3D-printed plastic holders and they are mounted in aluminium housings. Both housings have an opening above the SBD. The entire prototype can be seen in Figure 4. The photo shows the films with ^{10}B and LiF powder as the detector was tested for thermal neutron detection. The details of the electronic data acquisition system can be found in the literature [4, 17].

The relevant neutron reactions leading to the production of charged particles are ^{6}Li(n,t)α and

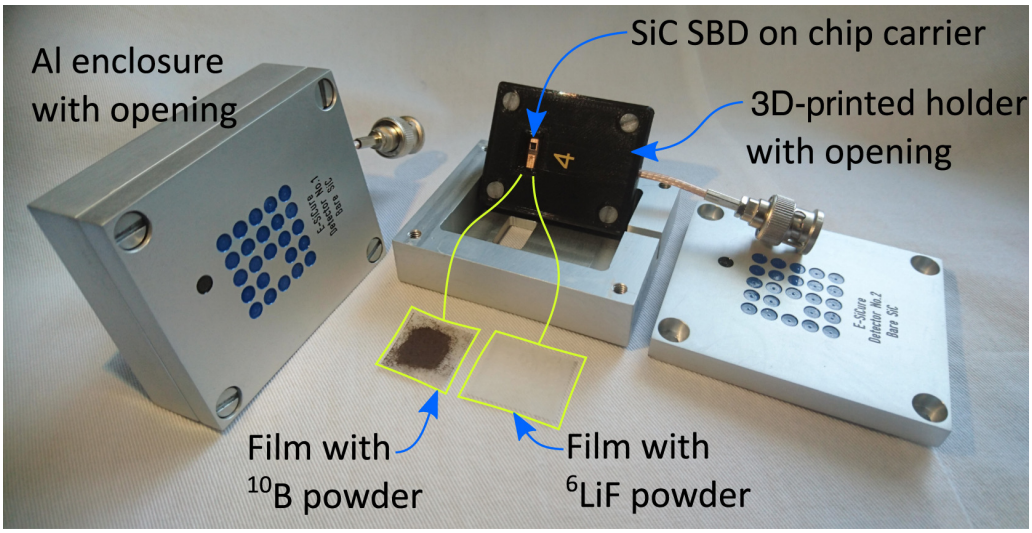

Figure 4. On the left there is an assembled detector prototype in aluminium enclosure. On the right prototype detector, the following components are displayed: SiC SBD mounted onto chip carrier with contacts, installed in 3D printed holder with opening, converter films (with ^{10}B and ^{6}LiF powder), open aluminium enclosure with lid. Picture from article [17].

^{10}B(n,α)^{7}Li, as mentioned earlier. The reaction involving ^{10}B has two branches with corresponding branching ratios (BR),

$$^{10}\mathrm{B}+ \longrightarrow \alpha(1776\ \mathrm{keV}) +^{7}\mathrm{Li}(1013\ \mathrm{keV});\ \mathrm{BR} = 6.3\ \%;\ \mathrm{Q} = 2789.5\ \mathrm{keV}, \tag{2}$$

$$^{10}\mathrm{B}+ \longrightarrow \alpha(1472\ \mathrm{keV}) +^{7}\mathrm{Li}^{*}(840\ \mathrm{keV});\ \mathrm{BR} = 93.7\ \%;\ \mathrm{Q} = 2311.9\ \mathrm{keV}, \tag{3}$$

where ^{7}Li* is an excited state of ^{7}Li and Q the reaction Q-value. The reaction with ^{6}Li is

$$^{6}\mathrm{Li}+ \longrightarrow \mathrm{t}(2731\ \mathrm{keV}) + \alpha(2052\ \mathrm{keV});\ \mathrm{Q} = 4783\ \mathrm{keV}. \tag{4}$$

In the experiments, the energies of the particles were recorded as an electrical signal or pulse with a specific energy, which was later categorised into bins to obtain a pulse-height spectrum. The pulse-height spectra were measured at various reactor power levels from 10 kW to 250 kW for both converter materials. Prior to the irradiations, a pulse-height vs. energy calibration was performed using an ^{241}Am surface source, emitting alpha particles at 5485.6 keV. In the recorded pulse-height spectra in Figure 5, some structures can be observed. These structures are attributable to the energies of the charged particles originating from the reactions (3) and (4). Using the notation from the article [4], the left spectrum in Figure 5 has five regions "R0-R4", the right spectrum has three regions "R0-R2" instead. The sharp peak appearing at low channel numbers is attributable to the electronic noise. Counts recorded at higher channel numbers (corresponding to higher energies) represent neutron detection events. In order to obtain representative values of the neutron sensitivity, total count rates were computed by applying an energy threshold of 600 keV, well above the observed peak R0 [17] to eliminate electronic noise.

An attempt was made to relate the regions of the spectra to the kinetic energies of the particles produced in the reactions. For the detector with a ^{10}B converter, R1 was connected to hits by ^{7}Li ions of energy $E = 1013$ keV and hits by ^{7}Li* ions of energy $E = 840$ keV, R2 was assigned to alpha particles with energies of $E = 1776$ keV or $E = 1472$ keV, R3 was assigned to a combined detection of alpha particles and ^{7}Li* from the dominant reaction, and R4 was attributed to the combined detection of alpha particles and ^{7}Li from the less likely reaction branch.

Overlaps are observed in areas without clear peaks, probably due to partial energy loss of the generated particles on the way to the detector (in the converter, in the air gap or in the front

contact). Another explanation is the limited resolution of the detection system. Regions were assigned based on the drops in the pulse-height spectra. Region R1 drops an energy of around 1000 keV, which corresponds to the maximum ^{7}Li energy of 1013 keV, and region R2 drops off at energies around 1700 keV, which corresponds to the maximum energy threshold of alpha particles (1776 keV). The maximum detectable particle energy from the dominant branch of the ^{10}B(n,α) reaction is 1472 keV + 840 keV = 2312 keV and corresponds to region R3. The fewest counts are found in region R4 and correspond to the maximum detectable particle energy from the less likely reaction (1776 keV + 1013 keV = 2789 keV).

When using the ^{6}LiF converter layer, the spectral properties could not be interpreted unambiguously. After preliminary analysis of the ^{10}B spectrum, the R1 region of the ^{6}LiF spectrum was attributed to partial energy deposition events. The R2 region was attributed to a combination of partial energy deposition by tritons (E = 2731 keV) and alpha particles (E = 2052 keV) [4].

An important property of a detector is the linear response. The linear response of the SiC prototype detector with a converter layer for thermal neutrons was demonstrated in the same experiment [17].

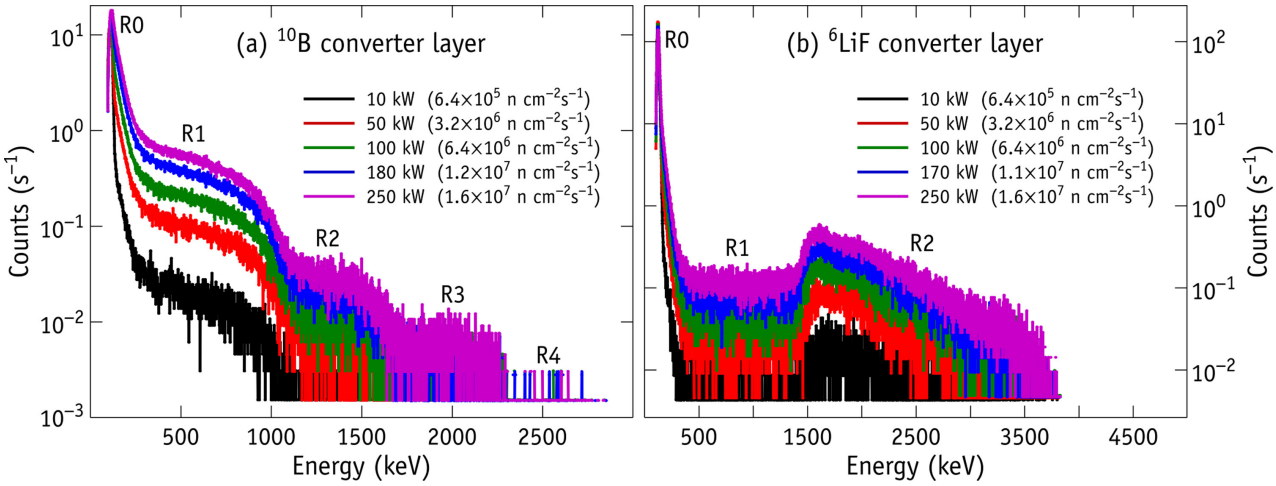

Figure 5. Measured count spectrum of SiC detectors covered with a ^{10}B converter (on the right) and covered with ^{6}LiF (on the left). The measurements were performed in the Dry chamber of the reactor at different power levels. Within the parentheses, the respective flux is written. Picture from article [4].

6. Summary

In this paper, I have given an overview of SiC neutron detectors, starting by explaining the importance of a detection technology other than that based on ^{3}He. The advantages of semiconductors and in particular the 4H polytype of silicon carbide were mentioned, with emphasis on radiation hardness and ease of fabrication. In Sections 2. and 4., I described the basic structure of a SiC Schottky barrier diode and the neutron converter layer.

In Section 3., I reviewed the key properties of SiC materials, such as polytypism. I described the crystalline structure of SiC typically used, 4H-SiC. The SiC band gap width and its dependence on polytypism was addressed. In terms of SBD quality, the easiest polytype to fabricate is the 4H-SiC polytype. A prototype SiC detector for thermal neutron detection was described in Section 5. It was shown that detectors based on SiC SBDs and equipped with thermal neutron converter films (enriched with ^{10}B and ^{6}LiF isotopes) clearly show neutron response.

This paper gives the reader insight into the reasons for pursuing new neutron detection technologies and the difficulties involved by presenting the best candidate material for SBD and the best materials for converters.

Future development of the SiC detector is currently being pursuit in the project e-SiCure 2, a collaboration of many parties including the JSI. The main goals of the project are developing and testing bigger sizes of SBDs, pixelated SBDs and converters for fast neutrons detection.

REFERENCES

[1] *A general monte carlo n-particle (mcnp) transport code*, Visited 3.3.2022 at 11.29.

[2] *Serpent - a monte carlo reactor physics burnup calculation code*, Visited 3.3.2022 at 11.29.

[3] W.J. Choyke, H. Matsunami, G. Pensl, and (Eds.), *Silicon Carbide: Recent Major Advances*, Advanced Texts in Physics (2004).

[4] José Coutinho, Vitor J.B. Torres, Ivana Capan, Tomislav Brodar, Zoran Ereš, Robert Bernat, Vladimir Radulović, Klemen Ambrožič, Luka Snoj, Željko Pastuović, Adam Sarbutt, Takeshi Ohshima, Yuichi Yamazaki, and Takahiro Makino, *Silicon carbide diodes for neutron detection*, Nuclear Instruments and Methods in Physics Research Section A: Accelerators, Spectrometers, Detectors and Associated Equipment **986** (2021), 164793.

[5] Brown DA, Chadwick MB, Capote R, Kahler A, Trkov A, Herman M, Sonzogni AA, Danon Y, Carlson AD, Dunn M, Smith DL, Hale GM, Arbanas G, Arcilla R, Bates CR, Beck B, Becker B, Brown F, Casperson RJ, Conlin J, Cullen DE, Descalle M, Firestone R, Gaines T, Guber K, Hawari AI, Holmes J, Johnson TD, Kawano T, Kiedrowski B, Koning AJ, Kopecky S, Leal L, Lestone J, Lubitz C, Mattoon CM, Mccutchan EA, Mughabghab SF, Mrquez Damin JI, Navratil P, Neudecker D, Nobre GPA, Noguere G, Paris M, Pigni MT, Plompen A, Pritychenko B, Pronyaev VG, Rochman D, Romano P, Roubtsov D, Schillebeeckx P, Simakov S, Sin M, Sirakov I, Sleaford B, Sobes V, Soukhovitskii E, Stetcu I, Talou P, Thompson I, Van Der Marck SC, Welser-Serrill L, White M, Wiarda D, Wormald JL, Wright RQ, Zerkle M, Zerovnik G, and Zhu Y, *Endf/b-viii.0: The 8th major release of the nuclear reaction data library with cielo-project cross sections, new standards and thermal scattering data*, NUCLEAR DATA SHEETS **148** (2018), 1–142.

[6] Wenkai Fu, Ryan G. Fronk, Douglas S. McGregor, and Jeremy A. Roberts, *Numerical evaluation of fast-sensitive microstructured semiconductor neutron detectors for treat hodoscope*, Nuclear Instruments and Methods in Physics Research. Section A, Accelerators, Spectrometers, Detectors and Associated Equipment **915** (2019).

[7] M. Hodgson, A. Lohstroh, P. Sellin, and D. Thomas, *Neutron detection performance of silicon carbide and diamond detectors with incomplete charge collection properties*, Nuclear Instruments and Methods in Physics Research Section A: Accelerators, Spectrometers, Detectors and Associated Equipment **847** (2017), 1–9.

[8] Richard T. Kouzes, James H. Ely, Luke E. Erikson, Warnick J. Kernan, Azaree T. Lintereur, Edward R. Siciliano, Daniel L. Stephens, David C. Stromswold, Renee M. Van Ginhoven, and Mitchell L. Woodring, *Neutron detection alternatives to 3he for national security applications*, Nuclear Instruments and Methods in Physics Research Section A: Accelerators, Spectrometers, Detectors and Associated Equipment **623** (2010), no. 3, 1035–1045.

[9] Lin-Yue Liu, Ling Wang, Peng Jin, Jin-Liang Liu, Xian-Peng Zhang, Liang Chen, Jiang-Fu Zhang, Xiao-Ping Ouyang, Ao Liu, Run-Hua Huang, and Song Bai, *The fabrication and characterization of ni/4h-sic schottky diode radiation detectors with a sensitive area of up to 4 cm2*, Sensors **17** (2017), no. 10.

[10] Gerhard Lutz, *Semiconductor radiation detectors*, Springer International Publishing AG, 2007.

[11] C Maples, G W Goth, and J Cerny, *Nuclear reaction q-values.*, Nucl. Data, Sect. A, 2: 429-612(Dec. 1966). (1966).

[12] F. Nava, G. Wagner, C. Lanzieri, P. Vanni, and E. Vittone, *Investigation of ni/4h-sic diodes as radiation detectors with low doped n-type 4h-sic epilayers*, Nuclear Instruments and Methods in Physics Research Section A: Accelerators, Spectrometers, Detectors and Associated Equipment **510** (2003), no. 3, 273–280.

[13] G. Nowak, M. Störmer, H.-W. Becker, C. Horstmann, R. Kampmann, D. Höche, M. Haese-Seiller, J.-F. Moulin, M. Pomm, C. Randau, U. Lorenz, R. Hall-Wilton, M. Müller, and A. Schreyer, *Boron carbide coatings for neutron detection probed by x-rays, ions, and neutrons to determine thin film quality*, Journal of Applied Physics **117** (2015), no. 3, 034901.

[14] Hajime Okumura, *Power electronics innovation by silicon carbide power semiconductor devices*, 2014 IEEE International Meeting for Future of Electron Devices, Kansai (IMFEDK), 2014, pp. 1–2.

[15] Se-Hwan Park, June-SiC Park, Hee-Seo, Seung Kyu Lee, Hee-Sung Shin, and Ho Dong Kim, *Development of sic detector for the harsh environment applications*, 2013 IEEE Nuclear Science Symposium and Medical Imaging Conference (2013 NSS/MIC), 2013, pp. 1–4.

[16] I. Porras, M. Sabaté-Gilarte, J. Praena, J.M. Quesada, and P.L. Esquinas, *33s for neutron capture therapy: Nuclear data for monte carlo calculations*, Nuclear Data Sheets **120** (2014), 246–249.

[17] Vladimir Radulović, Yuichi Yamazaki, Željko Pastuović, Adam Sarbutt, Klemen Ambrožič, Robert Bernat, Zoran Ereš, José Coutinho, Takeshi Ohshima, Ivana Capan, and Luka Snoj, *Silicon carbide neutron detector testing at the jsi triga reactor for enhanced border and port security*, Nuclear Instruments and Methods in Physics Research Section A: Accelerators, Spectrometers, Detectors and Associated Equipment **972** (2020), 164122.

[18] Lewis S. Ramsdell, *Studies on silicon carbide*, American Mineralogist **32** (1947), no. 1-2, 64–82.

[19] F.H. Ruddy, A.R. Dulloo, J.G. Seidel, S. Seshadri, and L.B. Rowland, *Development of a silicon carbide radiation detector*, IEEE Transactions on Nuclear Science **45** (1998), no. 3, 536–541.

[20] Varley F. Sears, *Neutron scattering lengths and cross sections*, Neutron News **3** (1992), no. 3, 26–37.

[21] S. Tripathi, C. Upadhyay, C.P. Nagaraj, A. Venkatesan, and K. Devan, *Towards radiation hard converter material for SiC-based fast neutron detectors*, Journal of Instrumentation **13** (2018), no. 05, P05026–P05026.

[22] S. Tripathi, Chandrakant Upadhyay, C. P. Nagaraj, K. Devan, A. Venkatesan, and K. Madhusoodanan, *Investigation of enhancement in planar fast neutron detector efficiency with stacked structure using geant4*, NUCL SCI TECH **28** (2017), no. 154.

[23] K Vasilevskiy and NG Wright, *Historical introduction to silicon carbide discovery, properties and technology*, Advancing Silicon Carbide Electronics Technology II: Core Technologies of Silicon Carbide Device Processing **69** (2020), 1.

[24] A. Žohar, V. Radulović, L.Snoj, R.Bernat, L. Bakrac, I. Capan, and T. Makino, *Silicon carbide neutron detector development-computational support with mcnp*, NENE (2021), no. 30.